

Comparison of three common inbred mouse strains reveals substantial differences in hippocampal GABAergic interneuron populations and in vitro network oscillations

Guersel Caliskan¹, Yunus Demiray¹, and Oliver Stork¹

¹Otto von Guericke Universitat Magdeburg

November 17, 2022

Abstract

A major challenge in neuroscience is to pinpoint neurobiological correlates of specific cognitive and neuropsychiatric traits. At the mesoscopic level, promising candidates for establishing such connections are brain oscillations that can be robustly recorded as local field potentials with varying frequencies in the hippocampus *in vivo* and *in vitro*. Inbred mouse strains show natural variation in hippocampal synaptic plasticity (e.g., long-term potentiation), a cellular correlate of learning and memory. However, their diversity in expression of different types of hippocampal network oscillations has not been fully explored. Here, we investigated hippocampal network oscillations in three widely used inbred mouse strains: C57BL/6J (B6J), C57BL/6NCrl (B6N) and 129S2/SvPasCrl (129) with the particular aim to identify common oscillatory characteristics in inbred mouse strains that show aberrant emotional/cognitive behaviour (B6N and 129) and compare them to “control” B6J strain. First, we detected higher gamma oscillation power in the hippocampal CA3 of both B6N and 129 strains. Second, an increased incidence of hippocampal sharp wave-ripple (SW-R) transients was evident in these strains. Third, we observed prominent differences in the densities of distinct interneuron types and CA3 associative network activity which are indispensable for sustainment of mesoscopic network oscillations. Together, these results supports the notion that *in vitro* hippocampal network oscillations, similar to classical plasticity read-outs measured in hippocampal slices, can be used as robust reductionist models to study electrophysiological correlates of emotional and cognitive phenotypes. Importantly, we add further evidence to profound physiological differences among inbred mouse strains commonly used in neuroscience research.

1. INTRODUCTION

Genetic variation is an important factor for individual variability in cognitive and neuropsychiatric traits (Deary *et al.* , 2009; Avshalom *et al.* , 2010; Ressler *et al.* , 2011). Specific inbred mouse strains provide useful models to study neurobiological correlates of such complex behavioural traits and their interaction with a certain genetic background. To date, while there is abundant evidence for altered emotional and cognitive phenotypes among widely used inbred mouse strains (Radulovic *et al.* , 1998; Stiedl *et al.* , 1999; Contet *et al.* , 2001; Rodgers *et al.* , 2002; Siegmund *et al.* , 2005; Bryant *et al.* , 2008; Camp *et al.* , 2009, 2012; Temme *et al.* , 2014; March *et al.* , 2014; Åhlgren & Voikar, 2019; Sloin *et al.* , 2022), electrophysiological correlates of such phenotypic characteristics are only limited to classical measurements of synaptic plasticity using hippocampal slice preparations (Nguyen, Abel, *et al.* , 2000; Nguyen, Duffy, *et al.* , 2000; Gerlai, 2002; Schimanski *et al.* , 2007; Freund *et al.* , 2016).

Of note, brain oscillations are thought to be involved in diverse emotional and cognitive functions (Buzsáki & Watson, 2012). Such oscillatory patterns with varying frequency ranges can be recorded robustly in the hippocampus *in vivo* and *in vitro* . Specifically, gamma oscillations (30-100 Hz) have been shown to support maintenance of working memory and attention (Fries *et al.* , 2001; Montgomery & Buzsáki, 2007). Their generation and sustainment primarily depend on the cholinergic level (Fisahn *et al.* , 1998; Vandecasteele

et al., 2014; Caliskan *et al.*, 2015). Accordingly, *in vivo* optogenetic activation of septo-hippocampal cholinergic fibres also triggers gamma oscillations in the hippocampus (Vandecasteele *et al.*, 2014). Importantly, “cholinergic” gamma-range oscillations can be induced in hippocampal slice preparations upon exposure to type 1 muscarinic acetylcholine (M1-) receptor agonists (Fisahn *et al.*, 1998). On the other hand, during reduced neuromodulation (e.g., slow wave sleep, quiet wakefulness) gamma oscillations are replaced by sharp wave-ripples (SW-R; (Buzsáki *et al.*, 1992; Ylinen *et al.*, 1995). These transient events occur at rate of 0.01-2 Hz together with superimposed fast ripples in the hippocampal CA1 (150-250 Hz) (Buzsaki, 1989; Ylinen *et al.*, 1995; Csicsvari *et al.*, 2000). Similarly, in slice preparations of ventral-to-mid hippocampus, spontaneous SW-R appear in the CA3 and propagate along the CA1/subiculum axis (Maier *et al.*, 2003; Maslarova *et al.*, 2015; Çalıřkan *et al.*, 2016). Convincing evidence indicates that these transients are involved in the reactivation of cellular activity patterns associated with a learning period and support both spatial and emotional memory consolidation (Wilson & McNaughton, 1994; Kudrimoti *et al.*, 1999; Girardeau *et al.*, 2017). Their targeted disruption impairs both spatial memory and contextual fear memory (Girardeau *et al.*, 2009; Wang *et al.*, 2015).

Most of the brain rhythms including gamma oscillations and SW-R are inhibition-based with complex involvement of different types of GABAergic interneurons that provide rhythmic inhibition to excitatory principal neurons (Hájos *et al.*, 2004; Hájos & Paulsen, 2009; Buzsáki & Watson, 2012). Among many different types of GABAergic interneurons, particular attention has been given to the involvement of parvalbumin-positive (PV+) and somatostatin (SST+) interneurons in generation and modulation of hippocampal network oscillations (Stark *et al.*, 2014; Norimoto *et al.*, 2018; Antonoudiou *et al.*, 2020). Notably, hippocampal CA3 subregion is able to generate robust oscillations due to strong recurrent collaterals among principal cells and their interaction with local interneurons forming an associative network (Le Duigou *et al.*, 2014).

To the best of our knowledge only a handful of studies have systematically investigated possible alterations in hippocampal network oscillations in inbred mouse strains with a main focus on gamma oscillations *in vitro* (Jansen *et al.*, 2009; Heistek *et al.*, 2010). Intriguingly, no previous work have explored hippocampal SW-R in common inbred mouse strains. Therefore, we studied hippocampal network oscillations in three commonly used inbred mouse strains: C57BL/6J (B6J), C57BL/6NCrl (B6N) and 129S2/SvPasCrl (129) with the goal to identify common oscillatory features in inbred mouse strains that show aberrant fear and anxiety (B6N and 129) and compare them to B6J strain. We further performed immunohistochemical analysis of main GABAergic interneuron populations and measured CA3 associative network activation using extracellular electrophysiology. We identified several common oscillatory features in B6N and 129 inbred mouse strains, however, with diverging interneuronal and CA3 associative network phenotypes. Our results suggest that *in vitro* hippocampal network oscillations can be used to study neurobiological correlates of phenotypic differences among common inbred mouse strains similar to previously reported classical measures of synaptic plasticity in hippocampal slices.

2. METHODS AND MATERIALS

2.1. Animals

Adult male JAX C57BL/6J (B6J), C57BL/6NCrl (B6N) and 129S2/SvPasCrl (129) mice were purchased from Charles River Laboratories at the age of eight-weeks old (Erkraht, Germany). Animals were allowed to acclimatize (group-housed; 3 to 5 mice per cage) to our in-house animal facility (inverted light-dark cycle) for at least 5 days before starting the experiments. All experiments were conducted in accordance with the European and German regulations for animal experiments and were approved by the local authorities (42502-2-1295 OvGMD). All experiments were performed during the dark phase.

2.2. Slice preparation and data acquisition

Mice were deeply anesthetized with isoflurane and decapitated. Brains were rapidly removed and placed in cold (4-8 C°) carbogenated (5% CO₂ / 95% O₂) artificial cerebrospinal fluid (aCSF) containing (in mM) 129 NaCl, 21 NaHCO₃, 3 KCl, 1.6 CaCl₂, 1.8 MgSO₄, 1.25 NaH₂PO₄ and 10 glucose. Slices that contain ventral-to-mid hippocampal formation and entorhinal cortex were obtained by cutting horizontal brain slices

at an angle of about 12deg in the fronto-occipital direction. Slices were transferred to an interface-type chamber perfused with aCSF at 32 \pm 0.5 degC (flow rate: 2.0 \pm 0.2 ml / min, pH 7.4, osmolarity \sim 300 mosmol / kg). Slices were incubated at least for one hour before commencing the recordings. Signals were pre-amplified using a custom-made amplifier and low-pass filtered at 3 kHz, after which they were sampled at a frequency of 5 kHz and stored on a computer hard disc for off-line analysis (Cambridge Electronic Design, Cambridge, UK).

2.3. Sharp wave-ripples

Glass electrodes (resistance in aCSF: 1-2 M Ω) were placed at pyramidal layer of CA3 and CA1. Data were recorded for \sim 5 min and 2 min artifact-free recordings were extracted as MATLAB files to be further analysed using a MATLAB-based code (MathWorks, Natick, MA). SW-R analysed as previously described (Çalişkan *et al.*, 2016). For detection of sharp waves (SW) the data was low-pass filtered at 45 Hz (Butterworth, 8th order). Three times the standard deviation (SD) of the low pass-filtered signal was used as the threshold for event detection. As a second criteria, the minimum interval between two subsequent SW was set to 80 ms. Data stretches of 125 ms centred to the maximum value of the SW event were stored for further analysis. For the analysis of the area under the curve of SW, the points crossing the mean of the data were used as the start and the end points of SW. The SW area was measured using trapezoidal numerical integration of low pass-filtered data. The raw data were band-pass-filtered at 120-300 Hz for analysis of the ripples that are superimposed to SWs (Butterworth, 8th order). Data stretches of 15 ms before and 10 ms after the maximum of SW event (25 ms) were stored for further analysis. Three times the standard deviation (SD) of the band-pass-filtered signal was used as the threshold for ripple detection. The analysis of the ripple amplitude was performed by triple-point-minimax-determination. Ripples were discarded from the analysis, if the difference between falling and rising component of a ripple was higher than 75%. Ripple frequencies were calculated only from subsequent ripples.

Network interactions between CA3 and CA1 during SW-R were analysed as previously described (Çalişkan *et al.*, 2016). Briefly, (1) CA3-CA1 propagation failure was calculated as the ratio of unconnected SW events in the CA3 and CA1 region within \pm 30 ms time-window; and (2) CA3-CA1 event correlation was analysed via measuring temporal relationship between presumably connected SW events in the CA3 and CA1. The global maximum correlation value within \pm 30 ms time-window was used for statistical comparison.

2.4. Cholinergic gamma oscillations

Prior to perfusion of slices with carbachol, the temperature of the recording chamber was increased to 35°C. After stable gamma oscillations were established (\sim 45-70 min carbachol perfusion), glass electrodes were placed at the pyramidal layer of CA3 and CA1 and data were recorded for \sim 5 min. Gamma oscillation were analysed with power spectra generated from artifact-free 2 min data by Fast Fourier Transformation using a frequency resolution of 0.8192 Hz using custom-made spike2 scripts (Cambridge Electronic Design, Cambridge, UK). Three parameters of the power spectra were extracted: 1) Peak frequency (Hz): the frequency value at the maximum power value. 2) Peak power (mV²): the power value at the maximum power. 3) Integrated power (mV²): the sum of power from 20 to 80 Hz. For further statistical analysis, power values were converted to log₁₀ values due to variable nature of gamma oscillation power in slice recordings. Furthermore, for local gamma correlations (CA3-CA3 or CA1-CA1 autocorrelations) and CA3-CA1 cross-correlations, correlograms were obtained from corresponding low-pass-filtered data (< 100 Hz) using Spike2 software. For local gamma correlations, the 2nd positive peak value of auto-correlations was used for further statistical analysis (See Fig. 1k). For the CA3-CA1 cross-correlation the peak value with lowest latency to time point 0 was used for further statistical comparison. As a cut off criteria for the CA3 recordings, slices with peak powers lower than 30 μ V², peak frequencies lower than 25 Hz and auto-correlation values lower than 0.1 were discarded. For the CA1 recordings the same criteria were used except the peak power criteria was lowered to 10 μ V² due to generally lower gamma oscillation strength observed in the CA1 in comparison to the CA3 subregion.

2.5. Evoked population spikes

Population spike responses from the CA3 and CA1 (the recording electrodes placed in the CA3 and CA1 pyramidal layers) were obtained via electrical stimulation using a bipolar tungsten electrode (Resistance in aCSF: ~ 0.1 M Ω) placed at the apical dendrites of the proximal CA1 stimulating the Schaffer collaterals. Such stimulation configuration leads to an antidromically evoked population spike in the CA3 pyramidal cell layer and a secondary orthodromic population spike via recurrent axon collaterals between CA3 pyramidal cells and between CA3 pyramidal cells and interneurons (Behrens *et al.* , 2005; Fano *et al.* , 2012; Çalıřkan *et al.* , 2015). The same stimulation leads to an orthodromic population spike in the CA1 pyramidal layer. An input-output (IO) curve was obtained using five intensities ranging from 10 μ A to 50 μ A. The population spike area was calculated by integrating the area above the of the population spike curve (mV.ms). Normalized collateral associative network activation in the CA3 was measured via dividing the antidromic population spike area to the orthodromic population spike area. Data analysis was performed off-line using Spike2 software (Version 8, Cambridge Electronic Design, Cambridge, UK).

2.6. Immunohistochemistry

Mice (6-8 mice per strain) were perfused transcardially with 4% Paraformaldehyde (PFA) in Phosphate-buffered saline (PBS), brains were removed and post-fixed in the same solution for 24 hours at 4 °C. For cryoprotection, they were further incubated with 30% sucrose/PBS for 48 hours. Brains were then snap-frozen, cut in 30 μ m thick horizontal sections in a Cryostat (Leica Biosystems) and slices were kept at 4°C in 0.02% sodium azide containing PBS until further processing. Slices were permeabilized and blocked in PBS containing 5% Donkey serum, 5% BSA and 0.3% TritonX for 1 hour. Rabbit anti-PV (1:500, ab11427, Abcam), rabbit anti-SST (1:250, sc13099, SantaCruz) and mouse anti-GAD67 (1:2500, MAB5406, Millipore) primary antibodies were used overnight at 4°C on corresponding slices. Slices were then incubated in donkey anti-rabbit Alexa-488 (1:1000, A21206, Invitrogen) or biotinylated goat anti-mouse (1:200, BA-9200, Vector Labs) secondary antibodies at room temperature for 2 hours. When biotinylated secondary antibody was used, antigen-antibody complexes were visualized by a final Streptavidin-Cy5 (1:1000, Invitrogen) incubation for 30 min at room temperature. Finally, slices were incubated in 300 nM working solution of DAPI in PB for 5 minutes as a nuclear stain and mounted on glass slides using Immu-Mount (Thermo Fischer Scientific). Images were acquired with DMI6000 epifluorescence microscope (Leica Microsystems) using 10x objective and tile-scan function. Three to six slices per mouse were used for cell number analyses in ImageJ (NIH). Hippocampal subregions (CA3 and CA1) were traced based on DAPI signal and corresponding regions were analysed for signal intensity specific to antigen-antibody complexes. To calculate cell numbers, Cell Counter plug-in of ImageJ was used and counted cells were cross-checked using the DAPI channel. Finally, cell number was first divided to the area of the traced regions and final values were normalized against the same measures obtained from the B6J mice.

2.7. Drugs

Carbachol was purchased from TOCRIS (Bristol, UK) and stock solutions were prepared in distilled water. Drugs were applied via continuous bath perfusion.

2.8. Statistical Comparison

Data are reported as mean \pm standard error of the mean (SEM). Number of slices (n) and number of animals (N) are indicated in the figure legends. Before performing statistical comparisons, data were checked for normality and equal variance using Shapiro-Wilk test and Levene's test, respectively. Statistical analysis of gamma oscillations, SW-R and interneuron counts were performed by one-way-ANOVA followed by posthoc comparison using Fisher LSD Method when data were normally distributed. For non-normal data, Kruskal-Wallis One Way Analysis of Variance on Ranks followed by posthoc comparison using Dunn's Method was used. The statistical comparison of IO curves between strains was performed by two-way repeated measures ANOVA followed by posthoc comparison using Fisher LSD Method with Greenhouse-Geisser correction (SigmaPlot for Windows Version 11.0, 2008 or GraphPad Prism, version 9, SD, California).

3. RESULTS

3.1. Increased sharp wave-ripple (SW-R) incidence in B6N and 129 mouse strain

Rodent acute brain slices obtained from the ventral-to-mid portion of the hippocampus spontaneously generate SW-R in the CA3-CA1 axis of the hippocampus (Figure 1a) (Maier *et al.*, 2003; Çalişkan *et al.*, 2016). Simultaneous local field potential recordings from CA3 and CA1 regions in slices of mouse strains B6J, B6N and 129 revealed substantial differences in the incidence and CA3-CA1 network interactions during SW-R (Figure 1b-f). We detected an increased incidence of CA3 SW (Figure 1c: $F(2,57)=4.457$, $p=0.016$) in the B6N substrain in comparison to 129 strain ($p=0.005$) while CA1 SW incidence (Figure 1d: $H(2)=13.413$, $p=0.001$) was significantly higher in both B6N ($p<0.05$) and 129 ($p<0.05$) mouse strains compared to B6J indicating a potential difference in CA3-CA1 communication during SW-R events. Indeed, propagation of SW events across CA3-CA1 regions (Figure 1e: $F(2,57)=6.419$, $p=0.003$) was more efficient in the 129 strain which exhibited much less propagation failures compared to other two strains (129 vs. B6J: $p<0.001$ and 129 vs. B6N: $p=0.049$). Moreover, correlation of co-occurring SW events in the CA3 and CA1 (Figure 1f: $F(2,57)=3.615$, $p=0.033$) were higher in the 129 ($p=0.016$) and B6N ($p=0.038$) strains in comparison to B6J strain. These results indicate that CA3-CA1 network interactions during SW-R are less efficient in the B6J substrain compared to other two strains evident by lower CA1 SW incidence and CA3-CA1 SW correlation.

Further analysis of SW-R characteristics revealed region-specific strain effects (Figure 1g-o). In the CA3, SW area (Figure 1h: $H(2)=12.837$, $p=0.002$) was significantly increased in B6N strain in comparison to other two strains (B6J vs. B6N: $p<0.05$, B6N vs. 129: $p<0.05$). No alterations were evident for signal-to-noise ratios (Figure 1i: $H(2)=0.290$, $p=0.865$). Ripple amplitudes (Figure 1j: $H(2)=7.390$, $p=0.025$) were significantly enhanced in the B6N compared to 129 ($p<0.05$) whereas ripple frequencies (Figure 1k: $H(2)=13.060$, $p=0.001$) were significantly lower in comparison to B6J ($p<0.05$) and 129 ($p<0.05$). In the CA1, SW area (Figure 1l: $H(2)=6.477$, $p=0.039$), signal-to-noise ratios (Figure 1m: $H(2)=7.119$, $p=0.028$) and ripple amplitudes (Figure 1n: $H(2)=12.452$, $p=0.002$) were significantly increased in B6N in comparison to B6J substrain ($p<0.05$ for all parameters). Lastly, no differences were detected in ripple frequencies (Figure 1o: $H(2)=3.084$, $p=0.214$). Together, both B6N and 129 strain appear to have increased propensity for SW-R generation/propagation whereas slices obtained from B6N seem to generate SW and ripples with larger amplitudes.

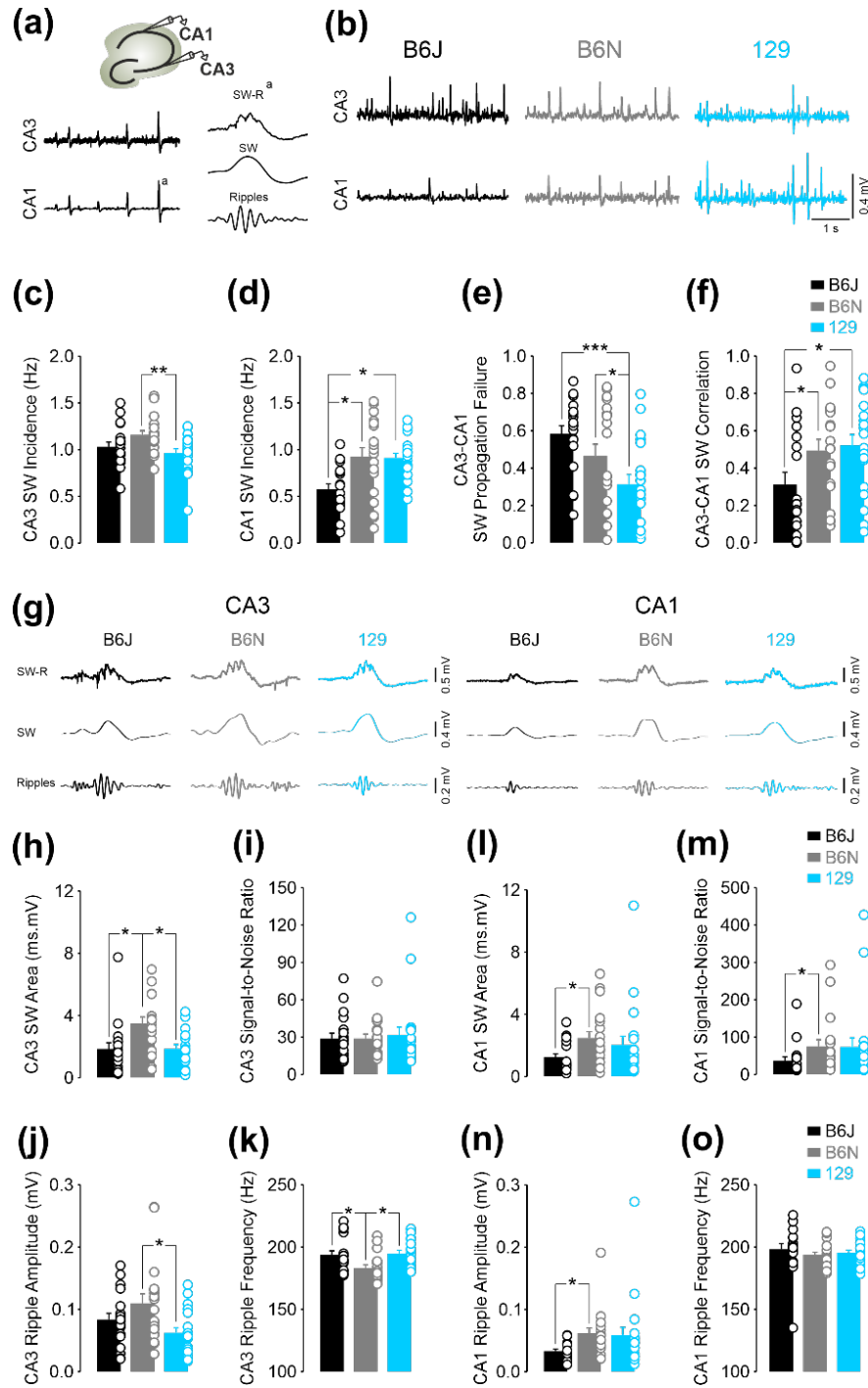


Figure 1. Enhanced sharp wave-ripples (SW-R) across CA3-CA1 hippocampal axis of B6N and 129 mouse strains. (a) Spontaneous SW-R were recorded from hippocampal CA3 and CA1 pyramidal layers. Representative local field potential recordings from the CA3 (top) and CA1 (down). An individual CA1 SW-R is marked, and low-pass-filtered SW (<45 Hz) and band-pass-filtered ripple (120-300 Hz) components are shown below. (b) Representative local field potential recordings from hippocampal CA3 and CA1 showing an increased SW incidence in CA1 subregion of B6N and 129 strains. Summary graphs (B6J:

N=7 mice, n=19 slices; B6N: N=7 mice, n=20 slices; 129, N=7 mice, n=20 slices) illustrating **(c)** increased CA3 SW incidence in B6N strain and **(d)** CA1 SW incidence in both B6N and 129 strains. Summary graphs showing **(e)** reduced propagation failure in 129 in comparison to other strains and **(f)** enhanced CA3-CA1 correlation during SW-R events in B6N and 129 compared to B6J. **(g)** Representative SW-R in CA3 and CA1 subregions for each mouse strain. SW-R were low-pass-filtered (<45 Hz) to isolate SW and band-pass-filtered (120-300) to isolate ripples. Summary data for CA3 subregion illustrating a significantly increased **(h)** SW area in B6N strain, **(i)** no change in signal-to-noise ratios, **(j)** enhanced ripple amplitudes in B6N in comparison to 129 and **(k)** reduced ripple frequencies in B6N in comparison to other strains. Summary data for CA1 subregion illustrating significantly enhanced **(l)** SW area, **(m)** signal-to-noise ratios, **(n)** ripple amplitudes in B6N in comparison to B6J substrain and **(o)** similar ripple frequencies across investigated strains. Statistical comparison for **(c)**, **(e)**, **(f)**: one-way-ANOVA followed by posthoc comparison using Fisher LSD Method. Statistical comparison for **(d)**, **(h)**, **(i)**, **(j)**, **(k)**, **(l)**, **(m)**, **(n)**, **(o)**: Kruskal-Wallis One Way Analysis of Variance on Ranks followed by posthoc comparison using Dunn's Method. Post-hoc statistical differences are indicated via * $p < 0.05$, ** $p < 0.01$ and *** $p < 0.001$. Data are presented \pm standard error of mean (SEM). Empty circles represent individual data points.

3.2. Augmented cholinergic gamma oscillations in B6N and 129 mouse strains

Non-selective cholinergic agonist carbachol (concentration range: 5-20 μ M) has been widely used to induce gamma oscillations with gamma peak frequencies around \sim 30-40 Hz (Figure 1a) (Fisahn *et al.*, 1998; Madencioglu *et al.*, 2021). In our experiments we perfused slices with 5 μ M carbachol for 45-70 min to induce prominent and stable gamma oscillations in an interface recording chamber. After our exclusion criteria, (see section 2.4. *Cholinergic gamma oscillations for details*), 57 recordings from CA3 (B6J: N=8 mice, n=24 slices; B6N: N=7 mice, n=14 slices; 129, N=7 mice, n=19 slices) and 44 recordings from CA1 (B6J: N=8 mice, n=18 slices; B6N: N=7 mice, n=13 slices; 129, N=7 mice, n=13 slices) were included in further analysis (Figure 2b).

In the CA3, the slices obtained from B6J substrain generated less prominent gamma oscillations (Figure 2c-e) that was evident by significantly lower integrated (20-80 Hz) gamma power (Figure 2d: $F(2,56)=6.201$, $p=0.004$) and gamma peak power (Figure 2e: $F(2,56)=6.160$, $p=0.004$) in comparison to both B6N substrain (Integrated Power: $p=0.004$; Peak Power: $p=0.002$) and 129 strain (Integrated Power: $p=0.006$; Peak Power: $p=0.016$). Interestingly, there was also a significant main effect for gamma peak frequency (Figure 2f: $H(2)=10.058$, $p=0.007$) with higher peak frequencies in slices obtained from 129 strain (B6J vs. 129: $p < 0.05$; B6N vs. 129: $p < 0.05$).

In the CA1, although a similar trend (Figure 2g-j) was evident no significant alterations were detected for integrated power (Figure 2h: $F(2,43)=3.089$, $p=0.056$). A similar decrease in peak gamma power in B6J strain was evident (Figure 2i: $F(2,43)=6.373$, $p=0.004$) in comparison to B6N substrain ($p < 0.001$) which remained only as a trend when compared to 129 strain (Peak Power: $p=0.057$). Similarly, slices obtained from 129 strain exhibited higher gamma peak frequencies (Figure 2j: $H(2)=12.166$, $p=0.002$) compared to other two strains (B6J vs. 129: $p < 0.05$; B6N vs. 129: $p < 0.05$).

Furthermore, we analysed gamma synchrony within and across CA3 and CA1 regions via computing auto- and cross-correlograms (Figure 2k). We detected an increased local gamma correlations in the CA3 (Figure 2l: $F(2,56)=3.959$, $p=0.025$) and CA1 (Figure 2m: $F(2,56)=5.129$, $p=0.010$) regions of B6N in comparison to B6J (CA3-CA3 correlation: $p=0.007$; CA1-CA1 correlation: $p=0.003$). Lastly, similar CA3-CA1 cross-correlations were calculated across three strains (Figure 2n: $H(2)=4.225$, $p=0.121$). Collectively, these data demonstrate that hippocampal slices obtained from B6J mouse strain express weaker cholinergic gamma oscillations in comparison to both B6N and 129 mouse strains.

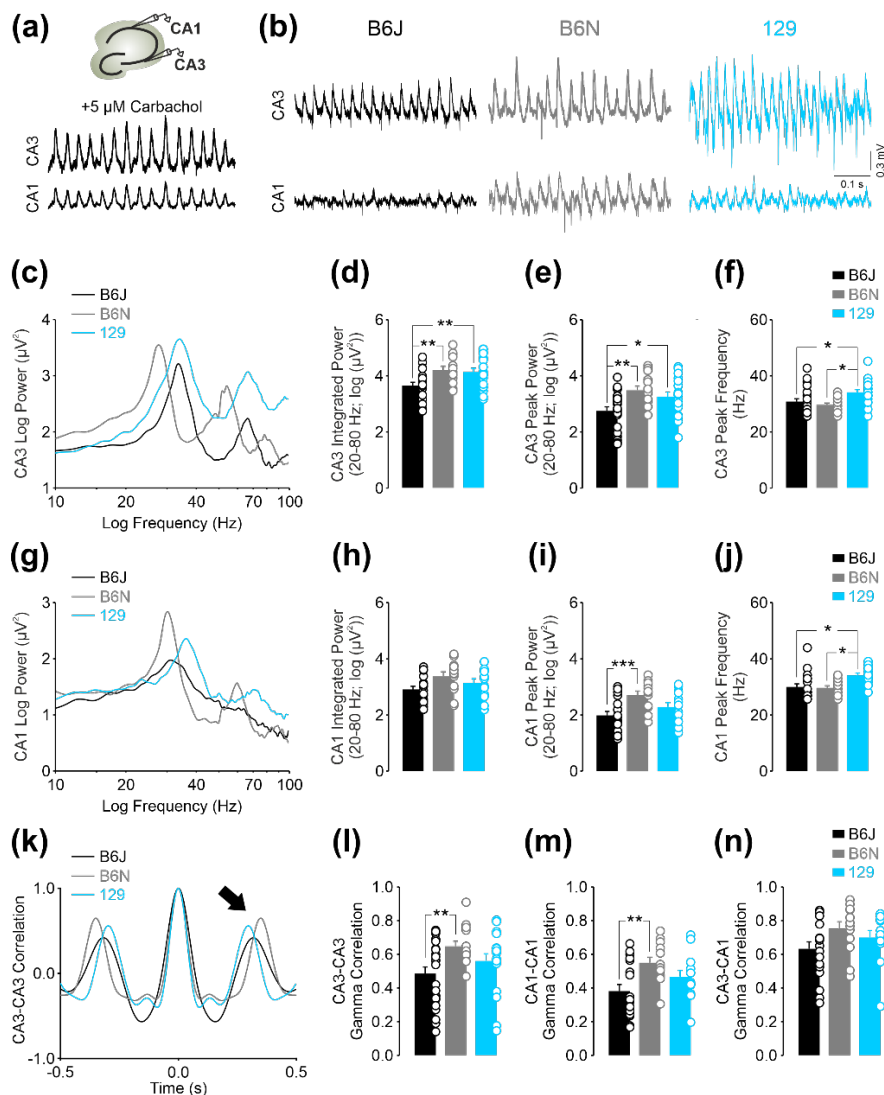


Figure 2. Augmented cholinergic gamma oscillations in B6N and 129 mouse strains. (a) Gamma oscillations were induced by perfusion of 5 μM carbachol and recorded from CA3 and CA1 pyramidal layers *in vitro*. (b) Representative cholinergic gamma oscillations in the CA3 and CA1. Note the augmented gamma oscillations in the B6N and 129 in comparison to B6J. (c) Representative power spectra of CA3 gamma oscillations (B6J: N=8 mice, n=24 slices; B6N: N=7 mice, n=14 slices; 129, N=7 mice, n=19 slices) from three strains. Note that to reduce the variability of gamma power *in vitro*, Log_{10} converted values are used. Summary graphs illustrating increased (d) gamma integrated power (20-80 Hz) and (e) gamma peak power in the B6N and 129 compared to B6J. (f) Summary graph showing a significant increase in gamma peak frequency of 129 in comparison to C57 sub-strains. (g) Representative power spectra of CA1 gamma oscillations from three strains (B6J: N=8 mice, n=18 slices; B6N: N=7 mice, n=13 slices; 129, N=7 mice, n=13 slices). Summary graphs illustrating (h) no significant alterations of integrated power (20-80 Hz) but (i) an enhanced peak power in B6N compared to B6J. (j) Summary graph showing a significant increase in gamma peak frequency of 129. (k) Representative auto-correlogram of CA3 gamma oscillations from three strains. Correlation peak values indicated by the arrow were further used for statistical comparison of local gamma correlations. Summary graphs showing enhanced (l) local CA3-CA3 (B6J: N=8 mice, n=24 slices; B6N: N=7 mice, n=14 slices; 129, N=7 mice, n=19 slices) and (m) CA1-CA1 gamma correlations (B6J:

N=8 mice, n=18 slices; B6N: N=7 mice, n=13 slices; 129, N=7 mice, n=13 slices) in B6N strain. **(n)** No statistical differences were detected for CA3-CA1 cross correlation of gamma oscillations (B6J: N=8 mice, n=18 slices; B6N: N=7 mice, n=13 slices; 129, N=7 mice, n=13 slices). Statistical comparison for **(d)**, **(e)**, **(h)**, **(i)**, **(l)**, **(m)**: one-way-ANOVA followed by posthoc comparison using Fisher LSD Method. Statistical comparison for **(f)**, **(j)**, **(n)**: Kruskal-Wallis One Way Analysis of Variance on Ranks followed by posthoc comparison using Dunn's Method. Post-hoc statistical differences are indicated via * $p < 0.05$ and ** $p < 0.01$. Data are presented \pm standard error of mean (SEM). Empty circles represent individual data points.

3.3. Reduced associative network activation in the CA3 of 129 mouse strain

Altered CA3 associative collateral network activation might underlie the differences in hippocampal network oscillations across studied mouse strains (Le Duigou *et al.*, 2014). For this purpose, we used antidromic stimulation of CA3 to generate a synaptically-mediated orthodromic population spike that follows a fast antidromic population spike (Figure. 3a-b; (Behrens *et al.*, 2005; Fano *et al.*, 2012). Comparison of IO curves for CA3 antidromic population spikes revealed a statistically significant stimulation strength x strain interaction (Figure 3c: $F(8,180)=2.936$, $p=0.004$) with a mild reduction of 129 antidromic responses in higher intensity ranges when compared to B6J substrain (See Figure 3c for posthoc comparisons). Interestingly, we detected a strong strain effect (Figure 3c: $F(2,45)=8.224$, $p < 0.001$) and stimulation strength x strain interaction (Figure 3d: $F(8,180)=3.173$, $p=0.002$) for orthodromic population spikes. Noteworthy, the orthodromic population spikes of 129 strain were profoundly reduced (See Figure 3d for posthoc comparisons). To assess the CA3 associative collateral network activation independent of antidromic stimulation we calculated normalized orthodromic responses via dividing orthodromic responses to corresponding antidromic responses across stimulation strengths and averaged these values within a slice (one data point per slice; see Figure 3e). Importantly, there was a strong strain effect (Figure 3e: $H(2)=9.201$, $p=0.01$) with a profound reduction in the normalized orthodromic responses in 129 strain when compared to B6J ($p < 0.05$). Using the same stimulation configuration, we recorded orthodromic population spikes in the CA1 (Figure 3f). However, we detected no difference between the strains (Figure 3g: $F(2,34)=0.183$, $p=0.833$). To sum up, these results demonstrate a differential recruitment of CA3 associative network across three strains with strong reduction in the 129 when compared B6J.

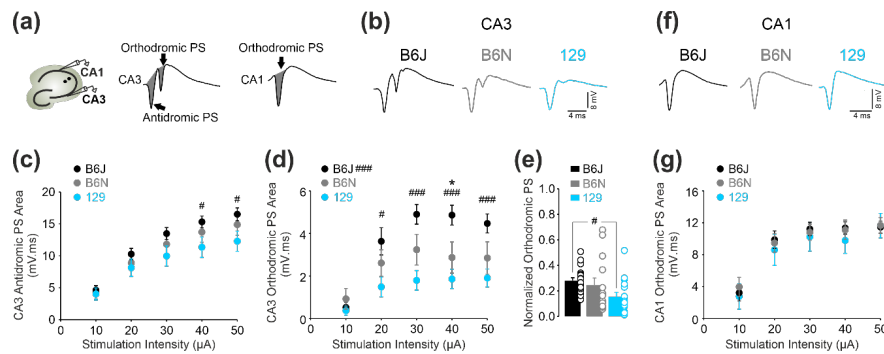


Figure 3. CA3 associative network activation differs across investigated mouse strains. (A) Hippocampal Schaffer collaterals were electrically stimulated, and evoked local field potential recordings were obtained from CA3 and CA1 pyramidal layers. Antidromic and orthodromic population spike (PS) areas (ms.mV) were calculated for stimulation intensities ranging from 0 to 50 μ A. **(b)** Representative antidromic and orthodromic population spikes in the CA3. Note the strong reduction of orthodromic responses in 129 mouse strain. CA3 IO curves (B6J: N=5 mice, n=18 slices; B6N: N=5 mice, n=14 slices; 129, N=5 mice, n=16 slices) **(c)** of antidromic and **(d)** orthodromic population spikes showing a slight reduction in antidromic population spikes and a strong reduction of orthodromic population spikes of 129 strains in comparison to B6J strain. **(e)** Reduced CA3 associative network activation in 129 mouse strain calculated via normalized orthodromic population spike responses. For this purpose, orthodromic responses were divided

to corresponding antidromic responses and were averaged across 5 stimulation strengths. **(f)** Representative orthodromic population spikes in the CA1. **(g)** CA1 IO curves (B6J: N=5 mice, n=13 slices; B6N: N=5 mice, n=12 slices; 129, N=5 mice, n=12 slices) showing similar population spike areas across investigated strains. Statistical comparison for **(c)**, **(d)**, **(g)**: two-way repeated measures ANOVA followed by posthoc comparison using Fisher LSD Method with Greenhouse–Geisser correction. Statistical comparison for **(e)**: Kruskal–Wallis One Way Analysis of Variance on Ranks followed by posthoc comparison using Dunn’s Method. Post-hoc statistical differences between strains B6J and 129 are indicated via # $p < 0.05$ and ### $p < 0.001$. Post-hoc statistical differences between substrains B6J and B6N are indicated via * $p < 0.05$. Data are presented \pm standard error of mean (SEM). Empty circles represent individual data points.

3.4. Altered GABAergic interneuron populations in the hippocampus of B6N and 129 strains

Inhibition mediated via hippocampal GABAergic interneurons is indispensable for generation and propagation of network oscillations along the hippocampal CA3–CA1 axis (Le Duigou *et al.*, 2014; Çalişkan *et al.*, 2016). Thus, we compared the number of three major population of interneurons (GAD67+, PV+ and SST+) in the hippocampal CA3 and CA1 subregions. Interestingly, a major strain effect was detected in the number of GAD67+ interneurons (Figure 4a-b) with a significant increase in both CA3 ($F(2,19)=40.627$, $p < 0.001$) and CA1 subregions ($F(2,19)=28.756$, $p < 0.001$) of 129 strain (For both CA3 and CA1: B6J vs. 129: $p < 0.001$, B6N vs. 129: $p < 0.001$).

Next, we observed a significant strain effect in the number of CA3 PV+ interneurons (Figure 3c-d: $F(2,19)=4.229$, $p=0.03$) with a significant reduction in the B6N strain in comparison to the other two strains (B6N vs. 129: $p=0.014$, B6N vs. B6J: $p=0.043$). Interestingly, the strain effect was further present in the CA1 subregion (Figure 3c-d: $F(2,19)=7.494$, $p=0.004$). Both B6N ($p=0.002$) and 129 ($p=0.009$) showed a significant reduction in comparison to B6J strain.

Last, a significant strain effect was detected in the number of CA3 SST+ interneurons (Figure 3e-f) with a significant increase in the 129 strain compared to the other mouse strains (B6J vs. 129: $p < 0.001$, B6N vs. 129: $p < 0.001$). No strain effect was found in the CA1 subregion ($F(2,20)=0.105$, $p=0.901$). These data demonstrate that 129 strain shows remarkable differences in the number of hippocampal interneurons in comparison to the C57/BL6 substrains in a cell-type-specific manner. Furthermore, there is a mild but significant change in the number of PV+ interneurons that are instrumental for generation of network oscillations, when C57/BL6 substrains are compared.

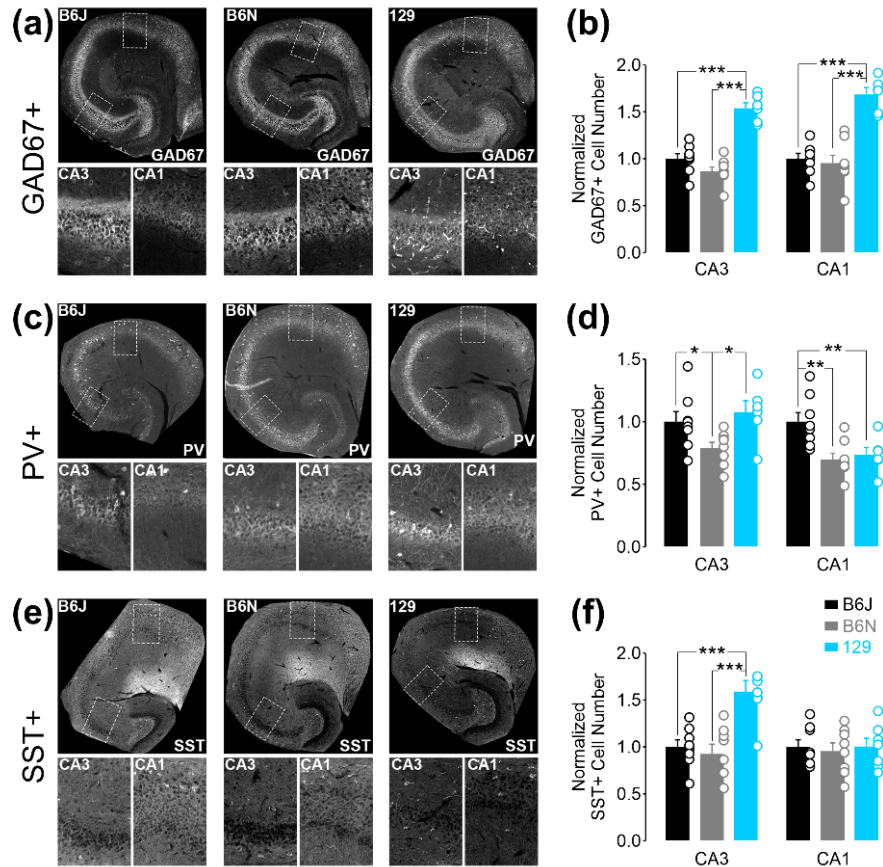


Figure 4. GABAergic interneuron populations are altered in the hippocampal CA3-CA1 axis across investigated mouse strains. (A) Representative hippocampal sections with immunohistochemical staining for glutamate decarboxylase (GAD)67. (b) Summary data (B6J: N=8 mice; B6N: N=8 mice; 129: N=6 mice) showing a significant increased number of GAD67+ interneurons in both CA3 and CA1 subregions of 129 mouse strain. (c) Representative hippocampal sections with immunohistochemical staining for parvalbumin (PV). (d) Summary data (B6J: N=8 mice; B6N: N=8 mice; 129: N=6 mice) showing a significant decrease in the CA3 and CA1 PV+ interneuron number of B6N strain. (e) Representative hippocampal sections for immunohistochemical staining for somatostatin (SST). (f) Summary data (B6J: N=8 mice; B6N: N=8 mice; 129: N=7 mice) showing a significant increase in CA3 SST+ interneuron number of 129 mouse strain. Statistical comparison for (b), (d), (f): one-way-ANOVA followed by posthoc comparison using Fisher LSD Method. Post-hoc statistical differences are indicated via *p<0.05, **p<0.01 and ***p<0.001. Data are presented \pm standard error of mean (SEM). Empty circles represent individual data points.

4. DISCUSSION

In the current study, we compared *in vitro* hippocampal network oscillations in three commonly used inbred mouse strains (B6J, B6N, 129) with the aim of elucidating common oscillatory patterns in inbred mouse strains that show aberrant emotional/cognitive behaviour (B6N and 129). We further investigated the density of main GABAergic interneurons in the hippocampal subregions and assessed hippocampal excitability via measuring population spikes in the CA3 and CA1 subregions. We identified three common oscillatory features in B6N and 129 strains that diverged from the B6J strain: (1) Larger amplitude cholinergic gamma oscillations in the CA3; (2) Higher incidence of CA1 SW with a specific increase of SW propagation along

the CA3-CA1 axis in the 129 strain; (3) Higher correlation of CA3 and CA1 SW transients. We further detected significant alterations in the number of specific inhibitory interneuron populations in the hippocampal subregions and activation of CA3 associative network that are essential for generation and maintenance of hippocampal network oscillations across three mouse strains. These observations align well with the notion that *in vitro* network oscillations provide useful reductionist models to investigate neurobiological underpinnings of phenotypic differences and highlight the importance of careful consideration of genetic background when designing experiments.

We used *in vitro* network oscillations that are dependent on the CA3 associative network activity as our experimental model. Hippocampal CA3 subregion forms an extensive associative network with abundant local recurrent excitatory connections that are under tight control of local inhibitory interneurons (Li *et al.* , 1994; Le Duigou *et al.* , 2014). These features make this circuit ideal for generation of local field potential network oscillations such as SW-R and gamma oscillations both *in vivo* and *in vitro* (Le Duigou *et al.* , 2014). Both oscillation types show similar features when recorded *in vitro* or *in vivo* (Butler & Paulsen, 2015; Çalıřkan & Stork, 2018). Indeed, there is accumulating evidence that *ex vivo* hippocampal network oscillations correlate with specific behaviours (Luet *et al.* , 2011; Çalıřkan *et al.* , 2016) or are modulated by behavioural manipulations (Albrecht *et al.* , 2013; Mizunuma *et al.* , 2014; Çalıřkan *et al.* , 2015) suggesting that our findings might be relevant for behavioural phenotypes observed in investigated inbred mouse strains.

In our study, B6J strain was used as control strain as it has been shown to exhibit normal spatial learning, normal anxiety levels, normal contextual fear memory and extinction (Gerlai, 1998a, 1998b, 2002; Stiedl *et al.* , 1999; Rodgers *et al.* , 2002; Siegmund *et al.* , 2005; Camp *et al.* , 2012; Åhlgren & Voikar, 2019). Of note, both B6N substrain and 129 strains have been consistently shown to exhibit aberrant contextual fear memory / extinction and elevated anxiety levels in comparison to B6J strain (Stiedl *et al.* , 1999; Rodgers *et al.* , 2002; Siegmund *et al.* , 2005; Camp *et al.* , 2012; Åhlgren & Voikar, 2019). We used hippocampal slices obtained from the ventral-to-mid portion of the hippocampus. Importantly, ventral hippocampus have been repeatedly shown to be involved in stress adaptation, emotional memory formation and anxiety, while the dorsal hippocampus is implicated in cognitive functions such as spatial memory processing (Kjelstrup *et al.* , 2002; Fanselow & Dong, 2010; Strange *et al.* , 2014). Therefore, our findings might be more relevant to emotional phenotypes observed in these two mouse strains.

Both B6N and 129 strains show significantly increased number of CA1 SW events and correlation of SW events in the CA3 and CA1 (Fig. 1). Additionally, 129 strain shows a facilitated propagation of SW events from CA3 to CA1 region. These findings aligns well with our previous work demonstrating that both increased propensity for SW-R generation in the ventral CA1 and increased SW propagation along CA3-CA1 axis correlate well with the aberrant fear extinction and persistent fear memories (Çalıřkan *et al.* , 2016). This is also supported by *in vivo* work showing causal involvement of SW-R in contextual fear memory consolidation (Wang *et al.* , 2015; Girardeau *et al.* , 2017; Ognjanovski *et al.* , 2017). Cholinergic hippocampal gamma oscillations (Fig. 2) are significantly enhanced in mice with anxious phenotype (B6N, 129) in comparison to a less anxious mouse strain (B6J). This observation also supports our previous study demonstrating reduced gamma oscillation in *ex vivo* slice preparations of mice with lower anxiety (Albrecht *et al.* , 2013). Indeed, heightened anxiety/emotionality appears to elicit increases of *in vivo* gamma oscillations in the ventral hippocampus and hypersynchronous gamma activity has been related to emotional psychopathologies (Headley & Paré, 2013; Dunkley *et al.* , 2014, 2015; Stujenske *et al.* , 2014). Future studies testing whether such oscillatory patterns are also observed *in vivo* are needed to substantiate these *in vitro* findings. Furthermore, it would be interesting to test whether cholinergic markers that are important for gamma generation (e.g., M1 receptors) are altered in these mouse strains.

Augmented network oscillations might be due to an altered CA3 associative collateral network activation in B6N substrain and 129 strain (Çalıřkan *et al.* , 2015). To assess the activation of CA3 associative collateral network (Fig. 3), we analysed antidromic population spikes and synaptically-mediated orthodromic population spikes triggered by antidromic stimulation of CA3 subregion (Behrens *et al.* , 2005; Fano *et al.* , 2012). We found no major effect on the antidromic population spikes in the CA3 subregion except for a minor

decrease in the 129 strain at higher stimulation strengths. However, the synaptically-mediated orthodromic population spikes were significantly reduced primarily in 129 strain. Local CA3 GABAergic interneurons control the excitation mediated by excitatory CA3-CA3 synapses (Li *et al.* , 1994; Le Duigou *et al.* , 2014). Thus, a reduction in the excitatory interactions within the CA3 recurrent collaterals might be due to an increased local inhibitory tonus in the 129 strain. Therefore, we analysed the expression of distinct markers for inhibitory interneurons that are crucial for generation and modulation hippocampal network oscillations (Fig. 4) (Mann *et al.* , 2005; Oren *et al.* , 2006; Ellender *et al.* , 2010). We used glutamate decarboxylase 67 (GAD67) as the pan-GABAergic marker. Furthermore, somatostatin (SST) and parvalbumin (PV) were used to quantify SST+ and PV+ interneuron populations. We observed a prominent overall increase in the number of GAD67+ interneurons in the hippocampal CA3-CA1 of 129 strain. This finding supports the notion that an increased inhibition might be present in the 129 strain which, in turn, can cause a reduction in the CA3 orthodromic population spikes for a given antidromic stimulation.

Changes in the number of interneuron populations can either cause the observed oscillatory features or reflect a compensatory mechanism. During both CA3 SW events and carbachol-induced gamma oscillation cycles, CA3 pyramidal cells receive a relatively stronger inhibitory input in comparison to an excitatory input (Oren *et al.* , 2006; Hajos *et al.* , 2013; Zemankovics *et al.* , 2013; Bazelot *et al.* , 2016). These compound intracellular excitatory/inhibitory events with a relatively stronger inhibitory component can be recorded as extracellular field potentials from the pyramidal cell layer as positive going voltage deflections (Bazelot *et al.* , 2010, 2016; Beyeler *et al.* , 2013). On the other hand, both perisomatic-region targeting PV+ interneurons and distal dendrite-targeting SST+ interneurons appear to receive relatively stronger excitation in comparison to inhibition during each gamma or SW event (Oren *et al.* , 2006; Hajos *et al.* , 2013; Pangalos *et al.* , 2013). Thus, a relatively increased inhibition during these oscillatory cycles can cause such an increase in gamma oscillation power as observed in the CA3 of both B6N and 129 strains.

Some evidence suggests that perisomatic inhibition onto pyramidal cells provided by PV+ basket cells is the source of gamma-range field potentials induced by carbachol (Gulyás *et al.* , 2010). Inconsistently, recent evidence shows a paradoxical increase in broadband gamma power in mice deficient for PV+ interneuron function, however, with reduced cellular synchronization to gamma oscillations (Guyon *et al.* , 2021). We observed a reduced PV+ interneuron number in both CA3 and CA1 of B6N strain. It is tempting to speculate that the reduction in PV+ interneuron number can cause the increased gamma power observed in the CA3 and CA1 of B6N strain. However, we detected an increased local gamma correlations in the CA3 and CA1 suggesting an increased gamma synchronization potentially mediated via increased PV+ interneuron functionality. Thus, as an alternative explanation, more efficient recruitment of PV+ interneurons by excitatory pyramidal cells could compensate for reduced PV+ interneuron abundance and increase perisomatic inhibition augmenting gamma field potential oscillations. Such increase in perisomatic inhibition can also lead to heightened SW amplitude as observed in the CA3 and CA1 of B6N strain. Furthermore, the reduction in the number of PV+ interneuron could alter the reciprocal interactions between PV+ interneurons during SW events that mediate the generation of fast ripple oscillations (Schlingloff *et al.* , 2014). In line, we observed a reduced CA3 ripple frequency in the B6N strain. Future studies assessing excitation-inhibition balance using intracellular recordings during field potential oscillations need to confirm whether such alterations are present in the B6N strain.

On the other hand, the increased number of SST+ interneurons observed in the hippocampus of 129 strain might underlie the increased gamma power. Indeed, a recent study suggests that SST+ interneurons are necessary for the maintenance of carbachol-induced gamma oscillations in hippocampal slices prepared similarly to our study (Antonoudiou *et al.* , 2020). Furthermore, the same study shows that optogenetic activation of SST+ interneurons leads to an increase in the peak frequency of cholinergic gamma oscillations *in vitro* . Indeed, in the 129 strain, the increased SST+ interneuron number was accompanied by faster gamma oscillation cycles evident by an increased peak frequency of gamma oscillations. However, it still remains to be elucidated how increased number of SST+ interneurons could directly affect the entrainment of pyramidal cells leading to augmented gamma oscillations as they mostly target the distal dendrites of the pyramidal neurons in the CA3 (Müller & Remy, 2014). Thus, it is likely that, during cholinergic gamma oscillations,

they modulate perisomatic inhibition via altering the excitability of principal neurons and spiking precision of PV+ interneurons as previously described for the dentate gyrus circuit (Savanthrapadian *et al.* , 2014). Alternatively, changes in the GABA-A receptor subunit composition might also underlie the alterations in the peak frequency of cholinergic gamma oscillations as previously described (Heistek *et al.* , 2010).

Taken together, we identified several common oscillatory and cellular features in the hippocampus of inbred mouse strains with aberrant emotional/cognitive phenotype (B6N and 129). Noteworthy, while there is substantial evidence for behavioural differences among C57/BL6 substrains (B6N vs. B6J), to the best of our knowledge, our study is the first to show potential interneuronal and oscillatory correlates of these differences in C57/BL6 substrains. Collectively, our study provides further evidence for altered hippocampal physiology among commonly used inbred mouse strains and cautions scientific community to consider genetic background as an important variable when designing experiments and interpreting their results.

ACKNOWLEDGEMENT

We are grateful to F. Blitz for the excellent work with the immunohistochemistry stainings; A. Koffi von Hoff and S. Stork for excellent technical assistance and to A. Bohnstedt and D. Al-Chackmakchie for excellent animal care.

STATEMENT OF ETHICS

All experiments were conducted in accordance with the European and German regulations for animal experiments and were approved by the Landesverwaltungsamt Saxony-Anhalt (42502-2-1295 OvGMD).

DISCLOSURE STATEMENT

The authors have no conflicts of interest to declare.

FUNDING INFORMATION

The work was supported by grants from the German Research foundation (STO488/6, CRC779/B05 and 362321501/RTG 2413 SynAGE to OS); Center for Behavioural Brain Sciences - CBBS promoted by Europäische Fonds für regionale Entwicklung - EFRE (ZS/2016/04/78113) and CBBS - ScienceCampus funded by the Leibniz Association (SAS-2015-LIN-LWC) to GC.

DATA AVAILABILITY STATEMENT

The data that support the findings of this study are available from the corresponding author upon reasonable request.

AUTHOR CONTRIBUTIONS

G.C. performed electrophysiological experiments, analysed data and wrote the first draft of the manuscript; Y.E.D. contributed substantially to the analysis and presentation of the immunohistochemistry data; O.S. and G.C. conceptualized the study and wrote the manuscript. All authors confirmed the last version of the manuscript.

References

- Åhlgren, J. & Voikar, V. (2019) Housing mice in the individually ventilated or open cages—Does it matter for behavioral phenotype? *Genes, Brain Behav.* , **18** , 1–12.
- Albrecht, A., Çalişkan, G., Oitzl, M.S., Heinemann, U., & Stork, O. (2013) Long-lasting increase of corticosterone after fear memory reactivation: Anxiolytic effects and network activity modulation in the ventral hippocampus. *Neuropsychopharmacology* , **38** .
- Antonoudiou, P., Tan, Y.L., Kontou, G., Upton, A.L., & Mann, E.O. (2020) Parvalbumin and Somatostatin Interneurons Contribute to the Generation of Hippocampal Gamma Oscillations. *J. Neurosci.* , **40** , 7668–7687.

- Avshalom, C., Hariri, A.R., Andrew, H., Uher, R., & Moffitt, T.E. (2010) Genetic sensitivity to the environment: The case of the serotonin transporter gene and its implications for studying complex diseases and traits. *Am. J. Psychiatry* , **167** , 509–527.
- Bazelot, M., Dinocourt, C., Cohen, I., & Miles, R. (2010) Unitary inhibitory field potentials in the CA3 region of rat hippocampus. *J. Physiol.* , **588** , 2077–2090.
- Bazelot, M., Teleńczuk, M.T., & Miles, R. (2016) Single CA3 pyramidal cells trigger sharp waves in vitro by exciting interneurons. *J. Physiol.* , **594** , 2565–2577.
- Behrens, C.J., van den Boom, L.P., de Hoz, L., Friedman, A., & Heinemann, U. (2005) Induction of sharp wave-ripple complexes in vitro and reorganization of hippocampal networks. *Nat. Neurosci.* , **8** , 1560–1567.
- Beyeler, A., Retailliau, A., Molter, C., Mehidi, A., Szabadics, J., & Leinekugel, X. (2013) Recruitment of Perisomatic Inhibition during Spontaneous Hippocampal Activity In Vitro. *PLoS One* , **8** .
- Bryant, C.D., Zhang, N.N., Sokoloff, G., Fanselow, M.S., Ennes, H.S., Palmer, A.A., & McRoberts, J.A. (2008) Behavioral differences among C57BL/6 substrains: Implications for transgenic and knockout studies. *J. Neurogenet.* , **22** , 315–331.
- Butler, J.L. & Paulsen, O. (2015) Hippocampal network oscillations — recent insights from in vitro experiments. *Curr. Opin. Neurobiol.* , **31** , 40–44.
- Buzsáki, G. (1989) Two-stage model of memory trace formation: A role for “noisy” brain states. *Neuroscience* , **31** , 551–570.
- Buzsáki, G., Horváth, Z., Urioste, R., Hetke, J., & Wise, K. (1992) High-frequency network oscillation in the hippocampus. *Science* , **256** , 1025–1027.
- Buzsáki, G. & Watson, B.O. (2012) Brain rhythms and neural syntax: implications for efficient coding of cognitive content and neuropsychiatric disease. *Dialogues Clin. Neurosci.* , **14** , 345–367.
- Çalışkan, G., Müller, I., Semtner, M., Winkelmann, A., Raza, A.S., Hollnagel, J.O., Rösler, A., Heinemann, U., Stork, O., & Meier, J.C. (2016) Identification of Parvalbumin Interneurons as Cellular Substrate of Fear Memory Persistence. *Cereb. Cortex* , **26** , 2325–2340.
- Caliskan, G., Schulz, S.B., Gruber, D., Behr, J., Heinemann, U., & Gerevich, Z. (2015) Corticosterone and corticotropin-releasing factor acutely facilitate gamma oscillations in the hippocampus in vitro. *Eur. J. Neurosci.* , **41** , 31–44.
- Çalışkan, G., Albrecht, A., Hollnagel, J.O., Rösler, A., Richter-Levin, G., Heinemann, U., & Stork, O. (2015) Long-term changes in the CA3 associative network of fear-conditioned mice. *Stress* , **3890** , 1–32.
- Çalışkan, G., Müller, I., Semtner, M., Winkelmann, A., Raza, A.S., Hollnagel, J.O., Rösler, A., Heinemann, U., Stork, O., & Meier, J.C. (2016) Identification of Parvalbumin Interneurons as Cellular Substrate of Fear Memory Persistence. *Cereb. Cortex* , **26** , 2325–2340.
- Çalışkan, G. & Stork, O. (2018) Hippocampal network oscillations as mediators of behavioural metaplasticity: Insights from emotional learning. *Neurobiol. Learn. Mem.* , **154** , 37–53.
- Camp, M., Norcross, M., Whittle, N., Feyder, M., D’Hanis, W., Yilmazer-Hanke, D., Singewald, N., & Holmes, A. (2009) Impaired Pavlovian fear extinction is a common phenotype across genetic lineages of the 129 inbred mouse strain. *Genes, Brain Behav.* , **8** , 744–752.
- Camp, M.C., MacPherson, K.P., Lederle, L., Graybeal, C., Gaburro, S., Debrouse, L.M., Ihne, J.L., Bravo, J.A., O’Connor, R.M., Ciocchi, S., Wellman, C.L., Lüthi, A., Cryan, J.F., Singewald, N., & Holmes, A. (2012) Genetic strain differences in learned fear inhibition associated with variation in neuroendocrine, autonomic, and amygdala dendritic phenotypes. *Neuropsychopharmacology* , **37** , 1534–1547.

- Contet, C., Rawlins, J.N.P., & Deacon, R.M.J. (2001) A comparison of 129S2/SvHsd and C57BL/6JOLAHsd mice on a test battery assessing sensorimotor, affective and cognitive behaviours: Implications for the study of genetically modified mice. *Behav. Brain Res.* , **124** , 33–46.
- Csicsvari, J., Hirase, H., Mamiya, a, & Buzsáki, G. (2000) Ensemble patterns of hippocampal CA3-CA1 neurons during sharp wave-associated population events. *Neuron* , **28** , 585–594.
- Deary, I.J., Johnson, W., & Houlihan, L.M. (2009) Genetic foundations of human intelligence. *Hum. Genet.* , **126** , 215–232.
- Dunkley, B.T., Doesburg, S.M., Jetly, R., Sedge, P.A., Pang, E.W., & Taylor, M.J. (2015) Characterising intra- and inter-intrinsic network synchrony in combat-related post-traumatic stress disorder. *Psychiatry Res. Neuroimaging* , **234** , 172–181.
- Dunkley, B.T., Doesburg, S.M., Sedge, P.A., Grodecki, R.J., Shek, P.N., Pang, E.W., & Taylor, M.J. (2014) Resting-state hippocampal connectivity correlates with symptom severity in post-traumatic stress disorder. *NeuroImage Clin.* , **5** , 377–384.
- Ellender, T.J., Nissen, W., Colgin, L.L., Mann, E.O., & Paulsen, O. (2010) Priming of hippocampal population bursts by individual perisomatic-targeting interneurons. *J. Neurosci.* , **30** , 5979–5991.
- Fano, S., Çalişkan, G., & Heinemann, U. (2012) Differential effects of blockade of ERG channels on gamma oscillations and excitability in rat hippocampal slices. *Eur. J. Neurosci.* , **36** .
- Fanselow, M.S. & Dong, H.W. (2010) Are the Dorsal and Ventral Hippocampus Functionally Distinct Structures? *Neuron* , **65** , 7–19.
- Fisahn, A., Pike, F.G., Buhl, E.H., & Paulsen, O. (1998) Cholinergic induction of network oscillations at 40 Hz in the hippocampus in vitro. *Nature* , **394** , 186–189.
- Freund, R.K., Graw, S., Choo, K.S., Stevens, K.E., Leonard, S., & Dell’Acqua, M.L. (2016) Genetic knockout of the $\alpha 7$ nicotinic acetylcholine receptor gene alters hippocampal long-term potentiation in a background strain-dependent manner. *Neurosci. Lett.* , **627** , 1–6.
- Fries, P., Reynolds, J.H., Rorie, a E., & Desimone, R. (2001) Modulation of Oscillatory Neuronal Synchronization by Selective Visual Attention. *Science (80-)* , **291** , 1560–1563.
- Gerlai, R. (1998a) A new continuous alternation task in T-maze detects hippocampal dysfunction in mice: A strain comparison and lesion study. *Behav. Brain Res.* , **95** , 91–101.
- Gerlai, R. (1998b) Contextual learning and cue association in fear conditioning in mice: a strain comparison and a lesion study. *Behav. Brain Res.* , **95** , 191–203.
- Gerlai, R. (2002) Hippocampal LTP and memory in mouse strains: Is there evidence for a causal relationship? *Hippocampus* , **12** , 657–666.
- Girardeau, G., Benchenane, K., Wiener, S.I., Buzsáki, G., & Zugaro, M.B. (2009) Selective suppression of hippocampal ripples impairs spatial memory. *Nat. Neurosci.* , **12** , 1222–1223.
- Girardeau, G., Inema, I., & Buzsáki, G. (2017) Reactivations of emotional memory in the hippocampus–amygdala system during sleep. *Nat. Neurosci.* , **20** , 1634–1642.
- Gulyás, A.I., Szabó, G.G., Ulbert, I., Holderith, N., Monyer, H., Erdélyi, F., Szabó, G., Freund, T.F., & Hájos, N. (2010) Parvalbumin-containing fast-spiking basket cells generate the field potential oscillations induced by cholinergic receptor activation in the hippocampus. *J. Neurosci.* , **30** , 15134–15145.
- Guyon, N., Zacharias, L.R., de Oliveira, E.F., Kim, H., Leite, J.P., Lopes-Aguiar, C., & Carlén, M. (2021) Network asynchrony underlying increased broadband gamma power. *J. Neurosci.* , JN-RM-2250-20.

- Hajos, N., Karlocai, M.R., Nemeth, B., Ulbert, I., Monyer, H., Szabo, G., Erdelyi, F., Freund, T.F., & Gulyas, A.I. (2013) Input-Output Features of Anatomically Identified CA3 Neurons during Hippocampal Sharp Wave/Ripple Oscillation In Vitro. *J. Neurosci.* , **33** , 11677–11691.
- Hájos, N., Pálhalini, J., Mann, E.O., Nèmeth, B., Paulsen, O., & Freund, T.F. (2004) Spike timing of distinct types of GABAergic interneuron during hippocampal gamma oscillations in vitro. *J. Neurosci.* , **24** , 9127–9137.
- Hájos, N. & Paulsen, O. (2009) Network mechanisms of gamma oscillations in the CA3 region of the hippocampus. *Neural Networks* , **22** , 1113–1119.
- Headley, D.B. & Paré, D. (2013) In sync: gamma oscillations and emotional memory. *Front. Behav. Neurosci.* , **7** , 170.
- Heistek, T.S., Timmerman, A.J., Spijker, S., Brussaard, A.B., & Mansvelder, H.D. (2010) Gabaergic synapse properties may explain genetic variation in hippocampal network oscillations in mice. *Front. Cell. Neurosci.* , **4** , 1–11.
- Jansen, R., Linkenkaer-Hansen, K., Heistek, T., Timmerman, J., Mansvelder, H.D., Brussaard, A.B., De Gunst, M., & Van Ooyen, A. (2009) Inbred mouse strains differ in multiple hippocampal activity traits. *Eur. J. Neurosci.* , **30** , 1092–1100.
- Kjelstrup, K.G., Tuvnes, F.A., Steffenach, H.-A., Murison, R., Moser, E.I., & Moser, M.-B. (2002) Reduced fear expression after lesions of the ventral hippocampus. *Proc. Natl. Acad. Sci.* , **99** , 10825–10830.
- Kudrimoti, H.S., Barnes, C.A., & McNaughton, B.L. (1999) Reactivation of hippocampal cell assemblies: effects of behavioral state, experience, and EEG dynamics. *J. Neurosci.* , **19** , 4090–4101.
- Le Duigou, C., Simonnet, J., Teleńczuk, M.T., Fricker, D., & Miles, R. (2014) Recurrent synapses and circuits in the CA3 region of the hippocampus: an associative network. *Front. Cell. Neurosci.* , **7** , 1–13.
- Li, X.-G., Somogyi, P., Ylinen, A., & Buzsáki, G. (1994) The hippocampal CA3 network: An in vivo intracellularly labeling study. *J. Comp. Neurol.* , **339** , 181–208.
- Lu, C.B., Jefferys, J.G.R., Toescu, E.C., & Vreugdenhil, M. (2011) In vitro hippocampal gamma oscillation power as an index of in vivo CA3 gamma oscillation strength and spatial reference memory. *Neurobiol. Learn. Mem.* , **95** , 221–230.
- Madencioglu, D.A., Çalışkan, G., Yuanxiang, P., Rehberg, K., Demiray, Y.E., Kul, E., Engler, A., Hayani, H., Bergado-Acosta, J.R., Kummer, A., Müller, I., Song, I., Dityatev, A., Kähne, T., Kreutz, M.R., & Stork, O. (2021) Transgenic modeling of Ndr2 gene amplification reveals disturbance of hippocampus circuitry and function. *iScience* , **24** , 102868.
- Maier, N., Nimmrich, V., & Draguhn, A. (2003) Cellular and network mechanisms underlying spontaneous sharp wave-ripple complexes in mouse hippocampal slices. *J. Physiol.* , **550** , 873–887.
- Mann, E.O., Suckling, J.M., Hajos, N., Greenfield, S.A., & Paulsen, O. (2005) Perisomatic feedback inhibition underlies cholinergically induced fast network oscillations in the rat hippocampus in vitro. *Neuron* , **45** , 105–117.
- March, A., Borchelt, D., Golde, T., & Janus, C. (2014) Differences in memory development among C57BL/6NCrl, 129S2/SvPasCrl, and FVB/NCrl mice after delay and trace fear conditioning. *Comp. Med.* , **64** , 4–12.
- Maslarova, A., Lippmann, K., Salar, S., R??sler, A., & Heinemann, U. (2015) Differential participation of pyramidal cells in generation of spontaneous sharp wave-ripples in the mouse subiculum in vitro. *Neurobiol. Learn. Mem.* , **125** , 113–119.

- Mizunuma, M., Norimoto, H., Tao, K., Egawa, T., Hanaoka, K., Sakaguchi, T., Hioki, H., Kaneko, T., Yamaguchi, S., Nagano, T., Matsuki, N., & Ikegaya, Y. (2014) Unbalanced excitability underlies offline reactivation of behaviorally activated neurons. *Nat. Neurosci.* , **17** , 503–505.
- Montgomery, S.M. & Buzsáki, G. (2007) Gamma oscillations dynamically couple hippocampal CA3 and CA1 regions during memory task performance. *Proc. Natl. Acad. Sci. U. S. A.* , **104** , 14495–14500.
- Müller, C. & Remy, S. (2014) Dendritic inhibition mediated by O-LM and bistratified interneurons in the hippocampus. *Front. Synaptic Neurosci.* , **6** , 1–15.
- Nguyen, P. V., Abel, T., Kandel, E.R., & Bourchouladze, R. (2000) Strain-dependent Differences in LTP and Hippocampus-dependent Memory in Inbred Mice. *Learn. Mem.* , **7** , 170–179.
- Nguyen, P. V., Duffy, S.N., & Young, J.Z. (2000) Differential Maintenance and Frequency-Dependent Tuning of LTP at Hippocampal Synapses of Specific Strains of Inbred Mice. *J. Neurophysiol.* , **84** , 2484–2493.
- Norimoto, H., Makino, K., Gao, M., Shikano, Y., Okamoto, K., Ishikawa, T., Sasaki, T., Hioki, H., Fujisawa, S., & Ikegaya, Y. (2018) Hippocampal ripples down-regulate synapses. *Science (80-)* , **359** , 1524–1527.
- Ognjanovski, N., Schaeffer, S., Wu, J., Mofakham, S., Maruyama, D., Zochowski, M., & Aton, S.J. (2017) Parvalbumin-expressing interneurons coordinate hippocampal network dynamics required for memory consolidation. *Nat. Commun.* , **8** , 15039.
- Oren, I., Mann, E.O., Paulsen, O., & Hájos, N. (2006) Synaptic currents in anatomically identified CA3 neurons during hippocampal gamma oscillations in vitro. *J. Neurosci.* , **26** , 9923–9934.
- Pangalos, M., Donoso, J.R., Winterer, J., Zivkovic, A.R., Kempter, R., Maier, N., & Schmitz, D. (2013) Recruitment of oriens-lacunosum-moleculare interneurons during hippocampal ripples. *Proc. Natl. Acad. Sci. U. S. A.* , **110** , 4398–4403.
- Radulovic, J., Kammermeier, J., & Spiess, J. (1998) Generalization of fear responses in C57BL/6N mice subjected to one- trial foreground contextual fear conditioning. *Behav. Brain Res.* , **95** , 179–189.
- Ressler, K.J., Mercer, K.B., Bradley, B., Jovanovic, T., Mahan, A., Kerley, K., Norrholm, S.D., Kilaru, V., Smith, A.K., Myers, A.J., Ramirez, M., Engel, A., Hammack, S.E., Toufexis, D., Braas, K.M., Binder, E.B., & May, V. (2011) Post-traumatic stress disorder is associated with PACAP and the PAC1 receptor. *Nature* , **470** , 492–497.
- Rodgers, R.J., Davies, B., & Shore, R. (2002) Absence of anxiolytic response to chlordiazepoxide in two common background strains exposed to the elevated plus-maze: Importance and implications of behavioural baseline. *Genes, Brain Behav.* , **1** , 242–251.
- Savanthrapadian, S., Meyer, T., Elgueta, C., Booker, S.A., Vida, I., & Bartos, M. (2014) Synaptic properties of SOM-and CCK-expressing cells in dentate gyrus interneuron networks. *J. Neurosci.* , **34** , 8197–8209.
- Schimanski, L.A., Ali, D.W., Baker, G.B., & Nguyen, P. V. (2007) Impaired hippocampal LTP in inbred mouse strains can be rescued by β -adrenergic receptor activation. *Eur. J. Neurosci.* , **25** , 1589–1598.
- Schlingloff, D., Kali, S., Freund, T.F., Hajos, N., & Gulyas, A.I. (2014) Mechanisms of Sharp Wave Initiation and Ripple Generation. *J. Neurosci.* , **34** , 11385–11398.
- Siegmund, A., Langnaese, K., & Wotjak, C.T. (2005) Differences in extinction of conditioned fear in C57BL/6 substrains are unrelated to expression of ??-synuclein. *Behav. Brain Res.* , **157** , 291–298.
- Sloin, H.E., Bikovski, L., Levi, A., Amber-Vitos, O., Katz, T., Spivak, L., Someck, S., Gattegno, R., Sivroni, S., Sjulson, L., & Stark, E. (2022) Hybrid Offspring of C57BL/6J Mice Exhibit Improved Properties for Neurobehavioral Research. *eneuro* , **9** , ENEURO.0221-22.2022.
- Stark, E., Roux, L., Eichler, R., Senzai, Y., Royer, S., & Buzsáki, G. (2014) Pyramidal Cell-Interneuron Interactions Underlie Hippocampal Ripple Oscillations. *Neuron* , **83** , 467–480.

- Stiedl, O., Radulovic, J., Lohmann, R., Birkenfeld, K., Palve, M., Kammermeier, J., Sananbenesi, F., & Spiess, J. (1999) Strain and substrain differences in context- and tone-dependent fear conditioning of inbred mice. *Behav. Brain Res.* , **104** , 1–12.
- Strange, B.A., Witter, M.P., Lein, E.S., & Moser, E.I. (2014) Functional organization of the hippocampal longitudinal axis. *Nat. Rev. Neurosci.* , **15** , 655–669.
- Stujenske, J.M., Likhtik, E., Topiwala, M.A., & Gordon, J.A. (2014) Fear and Safety Engage Competing Patterns of Theta-Gamma Coupling in the Basolateral Amygdala. *Neuron* , **83** , 919–933.
- Temme, S.J., Bell, R.Z., Pahumi, R., & Murphy, G.G. (2014) Comparison of inbred mouse substrains reveals segregation of maladaptive fear phenotypes. *Front. Behav. Neurosci.* , **8** , 1–9.
- Vandecasteele, M., Varga, V., Berényi, A., Papp, E., Barthó, P., Venance, L., Freund, T.F., & Buzsáki, G. (2014) Optogenetic activation of septal cholinergic neurons suppresses sharp wave ripples and enhances theta oscillations in the hippocampus. *Proc. Natl. Acad. Sci. U. S. A.* , **111** , 13535–13540.
- Wang, D. V, Yau, H.-J., Broker, C.J., Tsou, J.-H., Bonci, A., & Ikemoto, S. (2015) Mesopontine median raphe regulates hippocampal ripple oscillation and memory consolidation. *Nat. Neurosci.* , **18** , 728–735.
- Wilson, M.A. & McNaughton, B.L. (1994) Reactivation of hippocampal ensemble memories during sleep. *Science (80-.)* , **265** , 676–679.
- Ylinen, A., Bragin, A., Nádasdy, Z., Jandó, G., Szabó, I., Sik, A., & Buzsáki, G. (1995) Sharp wave-associated high-frequency oscillation (200 Hz) in the intact hippocampus: network and intracellular mechanisms. *J. Neurosci.* , **15** , 30–46.
- Zemankovics, R., Veres, J.M., Oren, I., & Hajos, N. (2013) Feedforward Inhibition Underlies the Propagation of Cholinergically Induced Gamma Oscillations from Hippocampal CA3 to CA1. *J. Neurosci.* , **33** , 12337–12351.

